Morphologies and Bridging Properties of Graft Copolymers

Liangshun Zhang, Jiaping Lin,* and Shaoliang Lin

Key Laboratory for Ultrafine Materials of Ministry of Education, School of Materials Science and Engineering, East China University of Science and Technology, Shanghai 200237, P. R. China

Received: August 4, 2006; In Final Form: November 2, 2006

Morphologies and bridging properties of graft copolymers in the bulk state were studied by using a real-space algorithm of self-consistent field theory in two dimensions. The phase transition from cylindrical to lamellar phase can be triggered by changing the position of graft points and the number of branches. The fraction of bridged conformation, f_{bridge}, shows a tendency to decrease with increasing the length of free end blocks, τ_1, and the number of branches, m. The value of f_{bridge} has a discontinuous drop when the transition from cylindrical to lamellar phase takes place. The relationship between m and the number of bridged chains per unit area, n_b, which is associated with the mechanical properties of copolymers, was also examined. It was found that n_b increases with increasing m in the cylindrical phase. However, in the lamellar phase, n_b decreases when m increases. It is proposed that the position of graft points and the number of branches are two important parameters for material design.

Downloaded via EAST CHINA UNIV SCIENCE & TECHLGY on October 22, 2020 at 07:45:17 (UTC).
See https://pubs.acs.org/sharingguidelines for options on how to legitimately share published articles.

Introduction

Molecular architecture has been recognized as an important role in determining morphologies, phase behavior, and material properties of copolymers. For the simplest AB diblock copolymer, the morphologies depend on the composition and the interaction between two different blocks.[1] Whereas, as the architecture of copolymer changes from diblock copolymer to graft copolymer, the morphological behavior depends not only on the composition and interaction energy, but also on the molecular architecture, like the position of junctions and the number of branches. Systematic studies of the relationship between molecular architecture and morphology were experimentally limited due to the unavailability of model graft copolymers with well-defined architecture. Gido et al. used the constituting block copolymer hypothesis to predict and interpret the morphological behavior of graft copolymers.[2−5] The constituting block copolymer hypothesis proposed that the morphological behavior of copolymers with a complex architecture is governed by the behavior of smaller block copolymer units (the constituting block copolymers) associated with the molecular architecture. It was concluded that the behavior of graft copolymers is dictated by the behavior of the smaller architectural subunits from which they are comprised. Other theoretical efforts have also been made to understand the influence of molecular architecture on the morphology and phase behavior of graft copolymers.[6−9] For example, the work of Balazs and her co-workers indicated that it is the χN of the average constituting single graft copolymer that determined the proximity of order−disorder transition for the graft copolymers (χ is the Flory−Huggins parameter and N is the total number of chemical segments in the single graft copolymer).[9] Recently, Ye et al. systematically studied the morphology and phase behavior of π-shaped copolymers via a combinatorial screening method based on self-consistent field theory (SCFT).[10] The transition of the order−order phase was investigated by varying the position of graft points. They predicted a hexagon−hexagon morphology that has not been reported for linear and star copolymers in the bulk state.

Morphological formation of A-*g*-B_m type graft copolymers has been investigated, and it was found that their microdomain structures were considered to be almost identical to A-*s*-B type star copolymers.[2−5] Despite the similarity of the domain structures between the graft and star copolymers, the backbone conformations of the A-*g*-B_m graft copolymers are different from those of the A-*s*-B star copolymers when backbone blocks form the continuous matrix. Star copolymers have only the free end blocks which adopt a dangled conformation. However, the backbone blocks of graft copolymers take either looped conformation whose junctions localize in the same domain or bridged conformation whose junctions are anchored on the different interfaces. The backbone blocks provide bridged "chains" across the continuous matrix that separates the discrete domains, thereby creating a physically cross-linked network between domains. When material is fractured, the bridged blocks must be pulled out of the microstructures, leading to a great deal of energy dissipation. A correlation between bridged blocks and mechanical strength in graft copolymers was experimentally demonstrated.[11−16] For example, Zhu et al. investigated morphological characteristics and mechanical properties of a series of graft copolymers, which exhibit high stress and strain at break.[15] It was proposed that the high strength of graft copolymers is attributed to bridged conformation of backbone in the microstructures. The blocks of backbone bridge adjacent domains, resulting in the enhanced mechanical properties. Thus, the fraction of bridged conformation is one of the fundamental issues in molecular design of graft copolymers that provides optimal mechanical properties.

There have already been a number of research efforts toward the bridging properties of linear block copolymer. Experimental efforts have been directed toward determining the bridging fraction by dielectrical techniques and rheological measurements.[17−20] A theoretical challenge to evaluate the bridging fraction was made by Matsen and Thompson.[21] They used the self-consistent-

* Address correspondence to this author. Phone: +86-21-64253370. Fax: +86-21-64253539. E-mail: jplinlab@online.sh.cn.

10.1021/jp0650432 CCC: $37.00 © 2007 American Chemical Society
Published on Web 12/21/2006

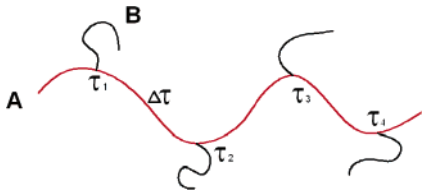

Figure 1. Molecular architecture of the graft copolymer.

field theory to evaluate the bridging properties of triblock copolymers with lamellar, cylindrical, and spherical morphologies, and the bridging fractions are about 40−50%, 60−65%, and 75−80%, respectively, which agreed with the results of experimental determination. Their calculation results also indicated that the bridging fraction depends weakly on the degree of segregation and the copolymer composition. Drolet and Fredrickson developed a real-space self-consistent algorithm for evaluating the bridging fraction of internal blocks in ABABA pentablock copolymers.[22] They anticipated that the pentablock copolymers with A-B-A-B-A composition of 10−15−50−15−10 in volume percentages should be optimally tough. Rasmussen et al. applied SCFT to calculate the bridging fraction of chain in (AB)*p* multiblock copolymer systems.[23] It was found that the bridging fraction has a sharp raise when polymerization index *p* goes from 2 to 3 and followed a slight decrease for copolymers with *p* more than 3. They also calculated the bridging fractions of the polymer chain that bridges consecutive lamellar domains. Daoulas et al. studied the bridging properties of styrene block copolymer self-adhesive materials by using self-consistent-field theory.[24] The SCFT results were combined with a slip tube model of rubber elasticity to predict the elastic behavior. Their predicted results were in good qualitative agreement with the experimental observations. These studies have focused on the limits of the linear block copolymers, whereas, as far as we know, a theoretical study of bridging properties for A-*g*-B$_m$ type graft copolymers has not been reported.

In this paper, we use a combination screening method based on the real-space implementation of the SCFT, developed by Fredricksion and co-workers,[22,25−28] to study the equilibrium microstructures assembled by graft copolymers in two-dimensional space. The average bridging fraction of backbone is evaluated by utilizing the equilibrium value of the mean fields obtained from the SCFT calculation in terms of the number of branches and the position of the first graft point. Our simulation results are useful for understanding the morphology−property relationship and optimizing the material performance.

Theory

We consider a system with volume V, containing n_G graft copolymers. Each copolymer is comprised of a flexible homopolymer **A** backbone along which m flexible homopolymer **B** grafts are spaced. The degrees of polymerization of the **A** and **B** chains are N_A and N_B, respectively. The volume fraction of **A**-type monomer in the system is denoted by f_A, and that of **B**-type monomer is $f_B = 1 - f_A$. A schematic representation of the architecture of graft copolymer is shown in Figure 1. The ith graft is located at τ_i given by

$$\tau_i = \tau_1 + \frac{(i-1)(1-2\tau_1)}{m-1} \qquad 1 \le i \le m \tag{1}$$

The length of blocks between neighbor junctions (in units of N_A) is denoted by $\Delta\tau = (1 - 2\tau_1)/(m - 1)$.

In the mean-field theory the configuration of the single copolymer chain is determined by a set of effective chemical potential fields $\omega_K(\mathbf{r})$ (K = A, B), replacing actual interchain interactions within the melt. These potential fields are conjugated to the monomer density fields $\varphi_K(\mathbf{r})$. We invoke an incompressibility ($\varphi_A(\mathbf{r}) + \varphi_B(\mathbf{r}) = 1$) by introducing a Lagrange multiplier $\zeta(\mathbf{r})$. For such an A-*g*-B$_m$ melt, the free energy per chain (in units of k_BT) is given by

$$F = -\ln\frac{Q_G}{V} - \frac{1}{V}\int d\mathbf{r}\,[\omega_A\varphi_A + \omega_B\varphi_B - \chi_{AB}N_G\varphi_A\varphi_B + \zeta(1 - \varphi_A - \varphi_B)] \tag{2}$$

where the Flory−Huggins parameter χ_{AB} characterizes the repulsive interaction between **A**- and **B**-type monomers, $N_G = N_A + mN_B$ denotes the total degree of polymerization of the graft copolymer, and $Q_G = \int d\mathbf{r}\, q_A(\mathbf{r},1)$ is the partition function for a single noninteracting, grafted chain subject to the fields $\omega_A(\mathbf{r})$ and $\omega_B(\mathbf{r})$ in terms of the backbone propagator $q_A(\mathbf{r},s)$. The contour length s increases continuously from 0 to 1 from one end of the homopolymer chain to the other. The spatial coordinate $\mathbf{r}$ is in units of R_g, where $R_g^2 = N_Ga^2/6$ (a is the statistical segment length). The backbone propagator is divided into $m + 1$ segments

$$q_A(\mathbf{r},s) = q_A^{(j)}(\mathbf{r},s) \tag{3}$$

$$\text{for } \tau_j \le s < \tau_{j+1};\ j = 0, 1, ..., m;\ \tau_0 \equiv 0,\ \tau_{m+1} \equiv 1$$

where each segment satisfies the modified diffusion equation

$$\frac{N_G}{N_A}\frac{\partial q_A^{(j)}(\mathbf{r},s)}{\partial s} = \nabla^2 q_A^{(j)}(\mathbf{r},s) - \omega_A(\mathbf{r})q_A^{(j)}(\mathbf{r},s) \tag{4}$$

and is subject to the following initial conditions:

$$q_A^{(j)}(\mathbf{r},\tau_j) = q_A^{(j=1)}(\mathbf{r},\tau_j)q_B(\mathbf{r},1);\ j = 1, 2, ..., m;\ q_A^{(0)}(\mathbf{r},0) = 1 \tag{5}$$

Here, $q_B(\mathbf{r},s)$ is a propagator for **B** graft that satisfies the following modified diffusion equation

$$\frac{N_G}{N_B}\frac{\partial q_B(\mathbf{r},s)}{\partial s} = \nabla^2 q_B(\mathbf{r},s) - \omega_B(\mathbf{r})q_B(\mathbf{r},s) \tag{6}$$

and is subject to the initial condition $q_B(\mathbf{r},0) = 1$ for the free end of the graft at $s = 0$. We also define a back-propagator of the jth **B** chain, $q_{Bj}^+(\mathbf{r},s)$. It satisfies eq 6 and starts on the end of the **B** chain tethered to the backbone. It is therefore subject to the initial condition

$$q_{Bj}^+(\mathbf{r},0) = \frac{q_A^{(j)}(\mathbf{r},\tau_j)q_A^{(j)}(\mathbf{r},1-\tau_j)}{q_B{}^2(\mathbf{r},1)} \tag{7}$$

In terms of these propagators, the monomer densities $\varphi_A(\mathbf{r})$ and $\varphi_B(\mathbf{r})$ become

$$\varphi_A(\mathbf{r}) = \sum_{i=1}^{m+1}\varphi_A^i(\mathbf{r}) = \frac{Vf_A}{Q_G}\sum_{i=1}^{m+1}\int_{\tau_{i-1}}^{\tau_i} ds\, q_A(\mathbf{r},s)q_A(\mathbf{r},1-s) \tag{8}$$

$$\varphi_B(\mathbf{r}) = \frac{Vf_B}{mQ_G}\sum_{j=1}^{m}\int_0^1 ds\, q_B(\mathbf{r},s)q_{Bj}^+(\mathbf{r},1-s) \tag{9}$$

where, $\varphi_A^i(\mathbf{r})$is the density coming from blocks between τ_{i-1} and τ_i. Finally, the minimization of the free energy, F, with respect to φ_A, φ_B, and ζ is achieved by satisfying the mean-field equations:

$$\omega_A(\mathbf{r}) = \chi_{AB}N_G\varphi_B(\mathbf{r}) + \zeta(\mathbf{r}) \quad (10)$$

$$\omega_B(\mathbf{r}) = \chi_{AB}N_G\varphi_A(\mathbf{r}) + \zeta(\mathbf{r}) \quad (11)$$

$$\varphi_A(\mathbf{r}) + \varphi_B(\mathbf{r}) = 1 \quad (12)$$

To solve the SCFT equations, we use a variant of the algorithm developed by Fredrickson and co-workers.[22,25−27] We start from a general random initial state. For the solution of the diffusion equations eq 4 and eq 6, we employed the Baker−Hausdorff operator splitting formula proposed by Rasmussen et al.[29,30] The density fields $\varphi_I(\mathbf{r})$ of species I, conjugated the chemical potential fields $\omega_I(\mathbf{r})$, are evaluated based on eqs 8 and 9 and eqs 10 and 11. The chemical potential fields $\omega_I(\mathbf{r})$ can be updated by using a two-step Anderson mixing scheme.[31]

Next, we briefly describe the calculation that determines the equilibrium properties of the backbone of the graft copolymer existing in bridged and looped conformations. Here, we consider A-*g*-B$_m$ graft copolymer melt in a region of the parameter space where the **A** blocks form the continuous matrix and the **B** blocks produce the cylindrical domains. The fraction of **A** blocks that bridge the neighbor **B** cylinders can be evaluated by utilizing the equilibrium configuration of fields ω_A and ω_B, obtained from the algorithm as previously described. The first step is to perform a Voronoi tessellation with respect to the center of a cylindrical domain. Next, we focus on a single Voronoi cell D_1. Following the approach of Matsen and Thompson,[21] the function is defined as

$$\bar{q}_A(\mathbf{r},s=\tau_i) = \begin{Bmatrix} q_A(\mathbf{r},s=\tau_i) & \mathbf{r} \in D_1 \\ 0 & \mathbf{r} \notin D_1 \end{Bmatrix} \quad (13)$$

constraining the *i*th graft point that belongs to D_1. The distribution can now be propagated by solving eq 4 as the initial condition at $s = \tau_i$ up to $s = \tau_{i+1}$.[32] The fraction, f_i, of looped conformation, where the blocks between the *i*th graft point and the (i+1)-th graft point have both ends in the cell D_1, is given by[24]

$$f_i = \frac{\int_{D_1} d\mathbf{r}\, \bar{q}_A(\mathbf{r},\tau_{i+1})q_A(\mathbf{r},1-\tau_{i+1})}{\int_V d\mathbf{r}\, \bar{q}_A(\mathbf{r},\tau_{i+1})q_A(\mathbf{r},1-\tau_{i+1})} \quad (14)$$

The average looped fraction, f_{loop}, for the cell D_1 is then obtained as

$$f_{loop} = \frac{1}{m-1}\sum_{i=1}^{m-1} f_i \quad (15)$$

The fraction of bridged conformation can be given by $f_{bridge} = 1 - f_{loop}$. An average value of f_{bridge} can be evaluated by repeating the calculation for all cells and performing an arithmetic average.

The different step of the evaluating procedure for the bridging fraction between the lamellar phase and the cylindrical phase is the Voronoi tessellation. It is preformed with respect to the interfaces of backbone-rich lamellar phase.

All simulations were carried out in two dimensions on a 64 × 64 lattice with periodic boundary conditions. Contour step sizes for the **A** backbone and **B** grafts were set at 0.01, respectively. The numerical simulations were carried up to a convergence of 10^{-6} in free energy and the achievement of the incompressibility condition. In the simulations the box was optimized for each system to minimize the free energy. The box size corresponding to the lowest free energy upon convergence was chosen as the most appropriate one.[33]

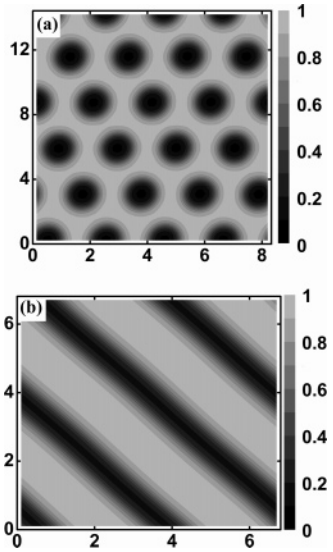

Figure 2. Total density field $\varphi_A(\mathbf{r})$ for a graft copolymer melt with $f_A = 0.70$ and $h = \chi_{AB}N_G/m = 20.0$: (a) $m = 2$, $\tau_1 = 0.05$, box size is $8.20R_g \times 14.20R_g$; (b) $m = 3$, $\tau_1 = 0.4$, box size is $6.70R_g \times 6.70R_g$.

Results and Discussion

In this work, we investigate the molecular architecture effect on the morphologies and bridging properties of graft copolymers. We focus on two factors: the number of branches and the block length between the neighbor junctions. With the constraint of the graft points τ_i (eq 1), the block length between the neighbor junctions can be determined only by the first junction τ_1. For example, if $\tau_1 = 0$, the first and last graft points are located at different ends of the backbone. If $\tau_1 = 0.5$, the graft copolymer becomes an A$_2$-*s*-B$_m$ star copolymer and the bridging fraction becomes zero. We restrict attention to graft copolymers with 70.0% backbone content. At this composition, the equilibrium morphology is predominantly a hexagonal array of cylinders in a continuous matrix rich in backbone blocks, while lamellar structure can also form under certain conditions. According to the work of Balazs and her co-workers,[9] we fix the interaction strength of the average constituting single graft copolymer $h = \chi_{AB}N_G/m$ at a value of 20.0, sufficient to produce microphase separation in the melt.

A typical total density field $\varphi_A(\mathbf{r})$ for graft copolymers with $m = 2$ and $\tau_1 = 0.05$ is shown in Figure 2a. The black (gray) areas represent the regions of lower (higher) density of **A**-type monomers. The graft blocks self-assemble into cylinders dispersed in a matrix rich in backbone blocks. According to the calculations, the cylindrical phase is observed over the range $0 \le \tau_1 \le 0.50$ with $m = 2$, $0 \le \tau_1 \le 0.38$ with $m = 3$, and $0 \le \tau_1 \le 0.33$ with $m = 4$. The cylindrical to lamellar phase transition takes place when the number of branches and position of the first graft point are changed. For example, the lamellar phase forms when $m = 3$ and $\tau_1 = 0.40$. The total density field $\varphi_A(\mathbf{r})$ of such a lamellar phase is shown in Figure 2b. The gray (black) color is assigned to the higher (lower) density of backbone blocks. The lamellar phase is produced over the range $0.38 < \tau_1 \le 0.50$ with $m = 3$, and $0.33 < \tau_1 \le 0.50$ with $m =$

4 in our calculations. Regarding the mechanism of the phase transition between the lamellar and the cylindrical phase when τ_1 and m are changed, it can be explained as follows. In the flat structure of a lamellar phase, the junctions of graft copolymers predominately localize along the same interface. When $\Delta\tau$ (length of blocks between neighbor junctions) increases, corresponding to a decrease in τ_1 or m, blocks between junctions become overcrowded. This results in more blocks stretching normal to the interface on the side of the backbone. The interfacial curvature could increase to alleviate this effect caused by the increase in $\Delta\tau$. As a result, the transition from the flat structure of a lamellar phase to the curved structure of a cylindrical phase occurs to lower the entropic contribution of the inner blocks to the overall free energy when $\Delta\tau$ increases.

Gido et al. used the constituting block copolymer hypothesis (CBCH) to predict and interpret the phase behavior of graft copolymers.[2−5] The phase behavior of graft copolymers is determined by the behavior of the constituting star copolymers associated with the architecture of graft copolymers. Existing Milner's theory is used to predict the phase behavior of the constituting star copolymers. In Milner theory, the phase behavior of the constituting star copolymers relies not only on the volume fraction of respective blocks, but also on the molecular asymmetry parameter.[6] Phase transition of the graft copolymers is predicted according to the variation of the molecular asymmetric parameter and the volume fraction of respective blocks.

The CBCH can predict the cylindrical to lamellar phase transition for the graft copolymers modeled in the present work under certain conditions. For example, when $\Delta\tau$ is asymptotically zero, the graft copolymer can be regarded as a star copolymer. The molecular asymmetry parameter of a symmetric star copolymer is given by $\epsilon = (n_B/n_A)(l_B/l_A)^{1/2}$, where n_i (i = A, B) is the arm number of the i-type block and l_i is the ratio of the segment volume to the square of the statistical segment length for the i block.[6] The A-*g*-B_2, A-*g*-B_3, and A-*g*-B_4 type graft copolymers can be regarded as A_2-*s*-B_2, A_2-*s*-B_3, and A_2-*s*-B_4 type star copolymers, respectively. The molecular asymmetry parameters of A_2-*s*-B_2, A_2-*s*-B_3, and A_2-*s*-B_4 copolymers are 1.0, 1.5, and 2.0, respectively. The CBCH predicts a cylindrical phase for A_2-*s*-B_2 and a lamellar phase for A_2-*s*-B_3 and A_2-*s*-B_4 with $f_A = 0.70$. In our simulations, the morphologies of A-*g*-B_2, A-*g*-B_3, and A-*g*-B_4 type graft copolymers are cylindrical, lamellar, and lamellar phase, respectively. The phase transitions predicted by CBCH upon changing the molecular structures agree well with our simulation results.

We subsequently investigate the conformation behavior of backbone in the bulk state. The looped, bridged, and dangled conformations of the backbone of graft copolymers in a cylindrical phase with **B** domains in an **A** matrix are shown in Figure 3a. The Voronoi tessellation is performed with respect to the centers of the domains. Similarly, the conformations of backbone in a lamellar phase are illustrated in Figure 3b. The Voronoi tessellation is preformed with respect to the interfaces of the **A**-rich lamellar phase. The free end blocks of the backbone dangle at the interfaces. The backbone blocks between the neighbor junctions are localized in the same Voronoi cell and form the looped conformation, while they are localized in the neighbor Voronoi cells and adopt the bridged conformation.

The bridging fraction f_{bridge} as a function of the position of the first graft point τ_1 for graft copolymers with number of branches $m = 2$, 3, and 4 is shown in Figure 4a. When $m = 2$, f_{bridge} versus τ_1 has a slight raise over the range $0.05 \le \tau_1 \le 0.10$, a slow drop over the interval $0.10 \le \tau_1 \le 0.33$, and a rapid drop as τ_1 increases beyond 0.33, whereas, when $m = 3$ and 4, f_{bridge} versus τ_1 only includes two regions: a slow drop and a rapid drop. For a given τ_1, f_{bridge} shows a decrease as m increases. To have a further insight into the bridging behavior, we also calculated the average distance between centers of the nearest-neighbor domains (shown in Figure 3a) as a function of τ_1, as shown in Figure 4b. There is a drop, a plateau, and a raise in the intercylinder spacing. When τ_1 is smaller, the intercylinder spacing is controlled by the $\Delta\tau$, the block length between neighbor junctions. With an increase in τ_1, the length of $\Delta\tau$ has shrunk and the distance D_{cyc} has dropped. Although the length of blocks, bridging the neighbor cylinders, has decreased, the bridging fraction has only a slow drop due to the intercylinder spacing being close. When τ_1 is larger, the free end blocks are the longest ones that control the distance between the neighbor cylinders. With further increase in τ_1, the

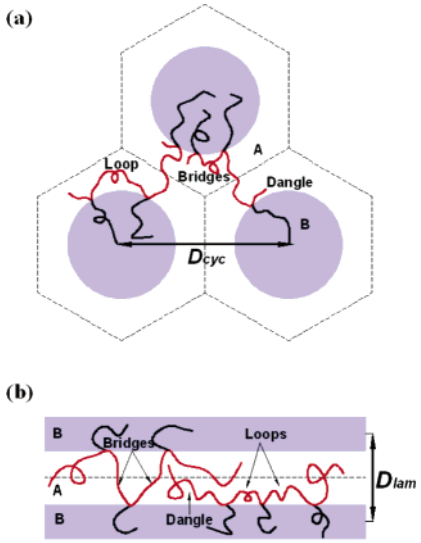

Figure 3. Typical conformations of A-*g*-B_m graft copolymers in (a) cylindrical phase with **B** domains in an **A** matrix and (b) lamellar phase. The looped, bridged, and dangled conformations are shown.

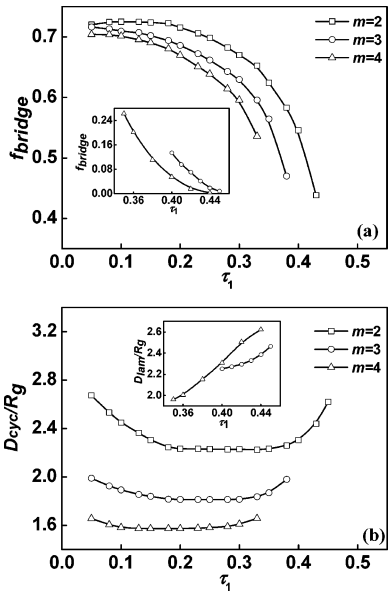

Figure 4. (a) bridging fraction f_{bridge} and (b) average distance D_{cyc} (in units of R_g) between the centers of the nearest-neighbor domains as a function of the position of the first graft point τ_1 for the graft copolymers with $m = 2$, 3, and 4. The inserts show f_{bridge} and D_{lam} as a function of τ_1 for graft copolymers with $m = 3$, 4.

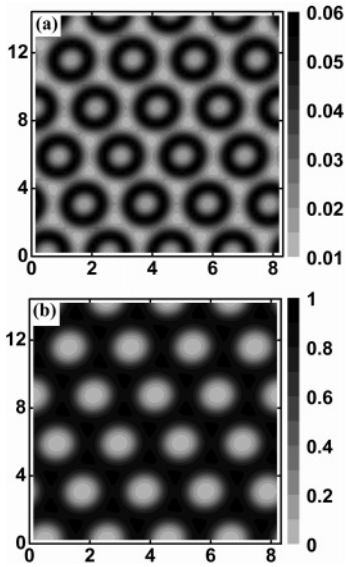

Figure 5. Density fields (a) $\varphi_A^1(\mathbf{r})$ of free end blocks and (b) $\varphi_A^2(\mathbf{r})$ of the backbone blocks between the junctions τ_1 and τ_2 for the graft copolymer with $m = 2$, $\tau_1 = 0.05$. Box size is $8.20R_g \times 14.20R_g$.

distance D_{cyc} has a raise and $\Delta\tau$ becomes shorter. As a result, the bridging fraction has a rapid drop. When τ_1 is intermediate, D_{cyc} is deep in the state with a big plateau of almost constant value due to the competition between the length τ_1 and $\Delta\tau$. The inserts of Figure 4 show the bridging fraction f_{bridge} and the average distance D_{lam} (shown in Figure 3b) as a function of τ_1 over the range $0.40 \le \tau_1 \le 0.45$ with $m = 3$, and $0.35 \le \tau_1 \le 0.44$ with $m = 4$, where the morphology transits from the cylindrical to the lamellar phase. There is a discontinuous change in the bridging fraction and the average distance at the phase transition. The value of f_{bridge} has a rapid drop and is asymptotically zero, but D_{lam} has a raise when τ_1 increases. These trends can be ascribed to the fact that free end blocks favoring looped conformation become long as τ_1 increases.

To achieve further understanding of the behavior of looped and bridged conformations, density fields $\phi_A^1(\mathbf{r})$ of free end blocks and $\phi_A^2(\mathbf{r})$ of the backbone blocks between the junction τ_1 and τ_2 have also been studied. Figure 5 shows a result for $m = 2$ and $\tau_1 = 0.05$, corresponding to the longer middle blocks. The total density field of **A** blocks is shown in Figure 2a. The black regions in Figure 5a,b represent the higher **A** volume fraction contributed from the free end blocks and middle blocks between τ_1 and τ_2, respectively. The free end blocks are localized along the interfaces of cylinders, while the middle blocks are concentrated in the continuous matrix rich in **A**-blocks. The calculation shows that 72.0% of the blocks adopt bridged conformation. When τ_1 increases to 0.43, corresponding to the longer free end blocks, the **A**-rich domain is predominantly the free end blocks and the interface regions contain the middle blocks, as shown in Figure 6, parts a and b, respectively. The free end blocks fill in the gap between the cylinders. The middle blocks between τ_1 and τ_2 reside in the interfacial regions, with only 43.8% of these blocks forming bridged conformation as revealed by the calculations. Thus, the shorter middle blocks are more favorable to adopt the looped conformation, while the longer middle blocks are more favorable to form the bridged conformation. As previously described, the lamellar phase is produced when $m = 3$ and $\tau_1 = 0.40$. The bridging fraction is 13.5%, which is lower than that in cylindrical morphology. The density fields $\phi_A^1(\mathbf{r})$ and $\phi_A^2(\mathbf{r})$ are shown in Figure 7. The

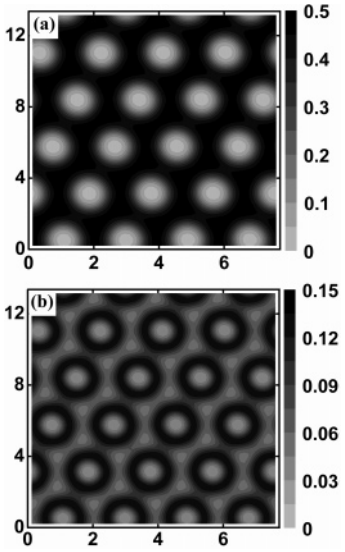

Figure 6. Density fields (a) $\phi_A^1(\mathbf{r})$of free end blocks, and (b) $\phi_A^2(\mathbf{r})$ of the backbone blocks between the junctions τ_1 and τ_2 for the graft copolymer with $m = 2$, $\tau_1 = 0.43$. Box size is $7.60R_g \times 13.16R_g$.

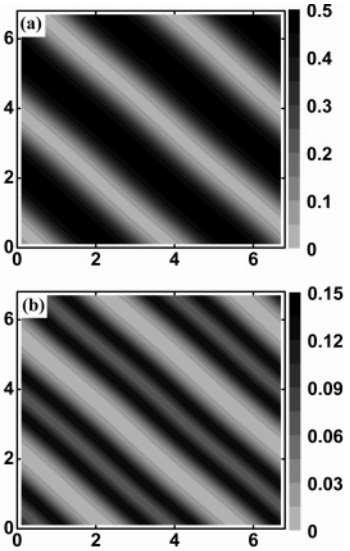

Figure 7. Density fields (a) $\phi_A^1(\mathbf{r})$ of free end blocks and (b) $\phi_A^2(\mathbf{r})$ of the backbone blocks between the junctions τ_1 and τ_2 for the graft copolymer with $m = 3$, $\tau_1 = 0.40$. Box size is $6.70R_g \times 6.70R_g$.

black areas represent the regions of higher densities of free end blocks (Figure 7a) and middle blocks between τ_1 and τ_2 (Figure 7b). Blocks between τ_1 and τ_2 reside in the interfacial area and broaden the interface.

The bridging behavior can be further viewed in Figure 8a in which f_{bridge} is plotted against the number of branches m for the graft copolymers with the position of the first graft point $\tau_1 = 0.10$, 0.15, and 0.20. With increasing the value of m, the bridging fraction sharply decreases and then remains almost constant when $\tau_1 = 0.10$, whereas there is always a decrease ascribed to the fact that the block length between neighbor junctions becomes shorter for $\tau_1 = 0.15$ and 0.20. As stated in the Introduction, the bridged chains of graft copolymers create a physically cross-linked network between neighbor domains, resulting in the enhanced mechanical properties. According to refs 19, 23, and 24, the tensile at the break is proportional to the number of bridged "chains" per unit area, $n_b = (m - 1)$-f_{bridge}, if the strength of the bridged "chains" is the same and

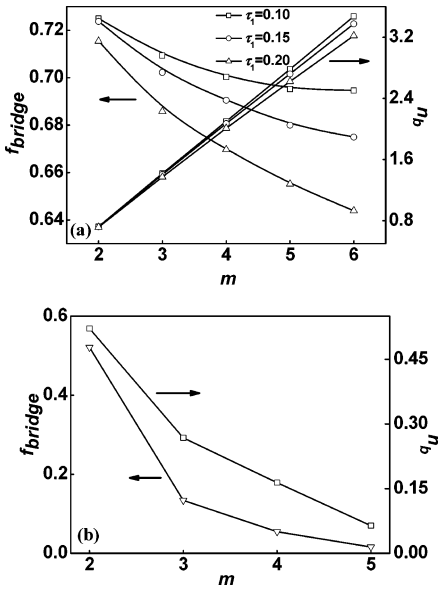

Figure 8. Bridging fraction (f_{bridge}) and number of bridged chains per unit area (n_b) as a function of the number of branches m with the position of the first graft point (a) $\tau_1 = 0.10$, 0.15, and 0.20 for the cylindrical phase and (b) $\tau_1 = 0.4$ for lamellar phase and cylindrical phase.

the "chains" are simultaneously pulled out. The higher value of n_b could lead to better mechanical properties. As shown in Figure 8a, the n_b increases with increasing the number of branches, and graft copolymers with smaller τ_1 values produce larger n_b. Therefore, the molecular architecture with larger m and smaller τ_1 should have optimal mechanical properties according to the above arguments. Weidisch et al. have experimentally investigated the tensile properties of graft copolymers comprised of polyisoprene (PI) backbone and polystyrene (PS) grafts.[14] It was found that strain and tensile strength at the break increase with increasing number of branches. The strain at the break is about 2300% for the graft copolymer sample with ten branches. Recently, Zhu et al. have investigated the effect of chain architecture on the tensile properties of a series of PI-*g*-PS graft copolymers and found the fact that tensile strength increases linearly with the number of junction points.[16] Therefore, our simulation results agree well with the general features of these experimental observations.

Next, we focus on f_{bridge} and n_b at the higher value of $\tau_1 = 0.40$, where the transition from the cylindrical to the lamellar phase takes place. The dependence of f_{bridge} and n_b on m is shown in Figure 8b (note that the graft copolymers form the cylindrical phase when $m = 2$; the bridging fraction of 0.52 is for the cylindrical phase). The bridging fraction becomes 0.13 when the cylindrical phase transforms to the lamellar phase ($m = 3$). A drop in the number of bridged chains per unit area also occurs due to the transition from the cylindrical to the lamellar phase. The values of f_{bridge} and n_b show a decrease as m further increases from 3 to 5. In such a case, the mechanical properties become worse when m increases. The above calculation results suggest that the position of graft points and the number of branches are two important parameters for controlling the mechanical properties of graft copolymers. On the other hand, although these predictions of self-consistent-field theory provide useful insight into the key features determining mechanical properties of graft copolymers, the connectivity between f_{bridge} and mechanical properties needs to build a more sophisticated model and consider more detailed information such as the interlocked entanglement.

Conclusions

Morphologies and bridging properties of graft copolymers in the bulk state were investigated by using the two-dimensional self-consistent-field theory. The graft copolymers exhibit cylindrical and lamellar mesostructures depending on the position of graft points and the number of branches. Studies on the chain conformation behavior of the backbone in the cylindrical phase revealed that f_{bridge} shows a tendency to decrease with increasing τ_1. When morphology transforms from the cylindrical to the lamellar phase, the value of f_{bridge} has a discontinuous drop and decreases rapidly as τ_1 increases. f_{bridge} and n_b as a function of m were also examined. It was found that f_{bridge} decreases with increasing m in both cylindrical and lamellar phases. n_b, which is associated with the mechanical properties of copolymers, increases with increasing m in the cylindrical phase. However, in the lamellar structure, n_b decreases when m increases.

Acknowledgment. This work was supported by the National Natural Science Foundation of China (20574018, 50673026). Support from the Doctoral Foundation of Education Ministry of China (Grant No. 20050251008), the Program for New Century Excellent Talents in University in China (NCET-04-0410), and the Project of Science and Technology Commission of Shanghai Municipality (05DJ14005) is also appreciated.

References and Notes

(1) Bates, F. S.; Fredrickson, G. H. *Phys. Today* **1999**, *52*, 32.
(2) Gido, S. P.; Lee, C.; Pochan, D. J.; Pispas, S.; Mays, J. W.; Hadjichristidis, N. *Macromolecules* **1996**, *29*, 7022.
(3) Xenidou, M.; Beyer, F. L.; Hadjichristidis, N.; Gido, S. P.; Tan, N. B. *Macromolecules* **1998**, *31*, 7659.
(4) Lee, C.; Gido, S. P.; Poulos, Y.; Hadjichristidis, N.; Tan, N. B.; Trevino, S. F.; Mays, J. W. *Polymer* **1998**, *39*, 4631.
(5) Beyer, F. L.; Gido, S. P.; Buschl, C.; Iatrou, H.; Uhrig, D.; Mays, J. W.; Chang, M. Y.; Garetz, B. A.; Balsara, N. P.; Tan, N. B.; Hadjichristidis, N. *Macromolecules* **2000**, *33*, 2039.
(6) Milner, S. T. *Macromolecules* **1994**, *27*, 2333.
(7) Olvera de la Cruz, M.; Sanchez, I. C. *Macromolecules* **1986**, *19*, 2501.
(8) Dobrynin, A. V.; Erukhimovich, I. Y. *Macromolecules* **1993**, *26*, 276.
(9) Shinozaki, A.; Jasnow, D.; Balazs, A. C. *Macromolecules* **1994**, *27*, 2496.
(10) Ye, X.; Shi, T.; Lu, Z.; Zhang, C.; Sun, Z.; An, L. *Macromolecules* **2005**, *38*, 8853.
(11) Kennedy, J. P.; Delvaux, J. M. *Adv. Polym. Sci.* **1991**, *38*, 141.
(12) Kennedy, J. P. In *Thermoplastic Elastomers*; Legge, N. R., Holden, G., Quirk, R., Schroeder, H. E., Eds.; Hanser: Munich, Germany, 1996.
(13) Peiffer, D. G.; Rabeony, M. *J. Appl. Polym. Sci.* **1994**, *51*, 1283.
(14) Weidisch, W.; Gido, S. P.; Uhrig, D.; Iatrou, H.; Mays, J. W.; Hadjichristidis, N. *Macromolecules* **2001**, *34*, 6333.
(15) Zhu, Y.; Weidisch, R.; Gido, S. P.; Velis, G.; Hadjichristidis, N. *Macromolecules* **2002**, *35*, 5903.
(16) Zhu, Y.; Burgaz, E.; Gido, S. P.; Staudinger, U.; Weidisch, R.; Uhrig, D.; Mays, J. W. *Macromolecules* **2006**, *39*, 4428.
(17) Watanabe, H. *Macromolecules* **1995**, *28*, 5006.
(18) Watanabe, H.; Sato, T.; Osaki, K.; Yao, M.; Yamagishi, A. *Macromolecules* **1997**, *30*, 5877.
(19) Takano, A.; Kamaya, I.; Takahashi, Y.; Matsushita, Y. *Macromolecules* **2005**, *38*, 9718.
(20) Takahashi, Y.; Song, Y.; Nemoto, N.; Takano, A.; Akazawa, Y.; Matsushita, Y. *Macromolecules* **2005**, *38*, 9724.
(21) Matsen, M. W.; Thompson, R. B. *J. Chem. Phys.* **1999**, *111*, 7139.
(22) Drolet, F.; Fredrickson, G. H. *Macromolecules* **2001**, *34*, 5317.
(23) Rasmussen, R. Ø.; Kober, E. M.; Lookman, T.; Saxena, A. *J. Polym. Sci. Part B: Polym. Phys.* **2003**, *41*, 104.
(24) Daoulas, K. Ch.; Theodorou, D. N.; Roos, A.; Creton, C. *Macromolecules* **2004**, *37*, 5093.
(25) Drolet, F.; Fredrickson, G. H. *Phys. Rev. Lett.* **1999**, *83*, 4317.
(26) Ganesen, V.; Fredrickson, G. H. *Europhys. Lett.* **2001**, *55*, 814.

(27) Fredrickson, G. H.; Ganesan, V.; Drolet, F. *Macromolecules* **2002**, *35*, 16.
(28) Patel, D. M.; Fredrickson, G. H. *Phys. Rev. E* **2003**, *68*, 051802.
(29) Tzeremes, G.; Rasmussen, R. Ø.; Lookman, L.; Saxena, A. *Phys. Rev. E* **2002**, *65*, 041806.
(30) Rasmussen, R. Ø.; Kalosakas, G. *J. Polym. Sci. Part B*: *Polym. Phys.* **2002**, *40*, 1777.
(31) Eyert, V. *J. Comput. Phys.* **1996**, *124*, 271.
(32) The boundary conditions were not used for the calculation of the bridging fraction due to the performance of the Voronoi tessellation. Therefore, the propagation $\bar{q}_A(\mathbf{r},s)$ was not accomplished with the Baker−Hausdorff operator splitting formula. It was calculated by the Crank−Nicolson algorithm.
(33) Bohbot-Raviv, Y.; Wang, Z. *Phys. Rev. Lett.* **2000**, *85*, 3428.